CDW GAP EFFECTS ON THE RAMAN SPECTRA IN ORTHORHOMBIC TaS_3

Shunji SUGAI

Department of Physics, Faculty of Science,
Osaka University, Toyonaka 560, Japan

Lattice vibrations in orthorhombic TaS_3 are investigated by polarized Raman scattering. Below the phase transition temperature of 218 K, satellite peaks become strong on the lower-energy slopes of the broad peaks which are dominant at room temperature. The decrease of the dominant peak below T_c is attributed to the decrease of the scattering probability from the intraband process in the chain with a large CDW gap, with the assumption that the interchain interaction is weak and the satellite peaks are due to the same normal modes of 24 chains in the unit cell.

I. Introduction

Transition metal trichalcogenides are typical one dimensional materials. Metallic compound TaS_3 shows charge density wave (CDW) phase transition at 218 K.[1] Two types of crystal structures are known in the normal phase of TaS_3. One is an orthorhombic structure[2] and the other is a monoclinic structure.[3] Though the space group of the orthorhombic structure had been reported to be $C222_1$ (D_2^5), a recent experiment by the convergent-beam electron diffraction method revealed the $Pmn2_1$ (C_{2v}^7) symmetry[4] at room temperature. The dimensions of the unit cell are a=36.804, b=15.177, and c=3.340 Å (chain direction), including 24 trigonal prismatic chains. Below the phase transition temperature the superlattice of 2a × 8b × 4c is formed.[5] Electron and x-ray diffraction experiments[1,5-7] have been performed for the crystallographic investigation. The lattice vibrations were investigated by Tsang et al.[8] by means of Raman scattering. Transport experiments[1,9-15] revealed the metal to semiconductor transition near the T_c. The non-Ohmic conductivity and the current noise, which are attributed to the collective sliding motion of the CDW, have been observed in TaS_3[16-18] as well as $NbSe_3$.

II. Experimental results

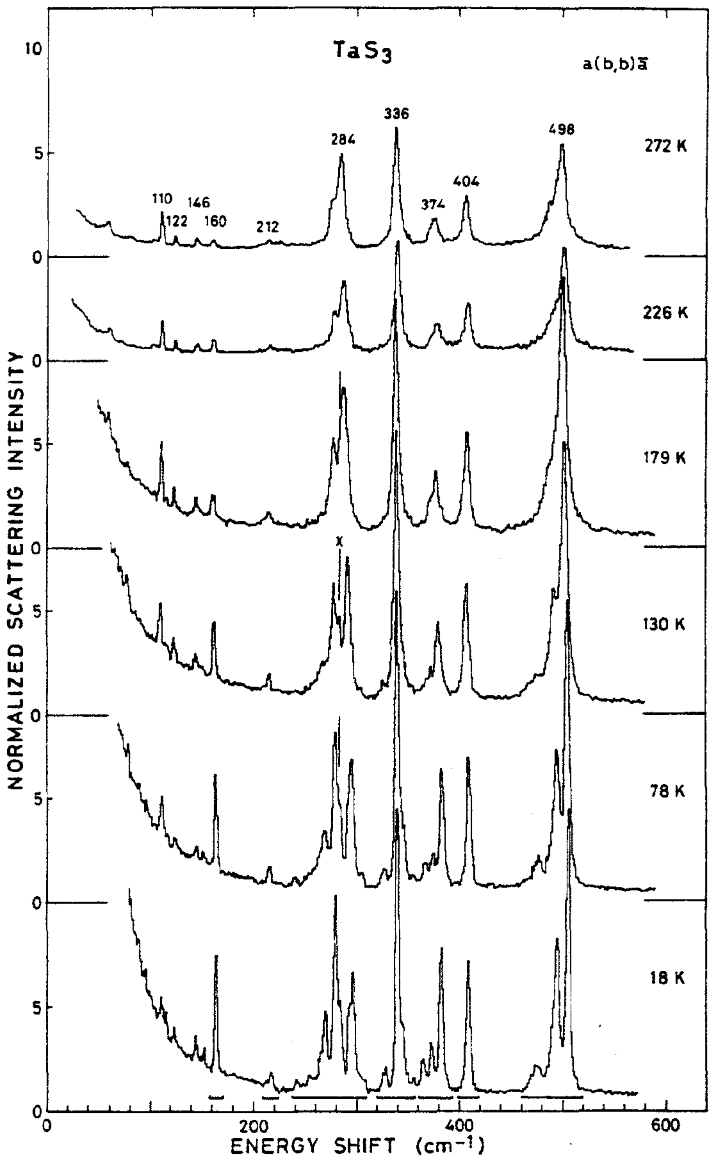

Fig. 1. Raman spectra of TaS_3 in the a(b,b)ā polarization configuration.

The Raman scattering experiment was made on the single crystal of orthorhombic TaS_3 by the use of a 5145 Å Ar-ion laser. The typical size of the crystals was 15μm × 40μm × 5mm. Figures 1, 2, and 3 show the Raman spectra in the a(b,b)ā, a(c,c)ā, and a(c,b)ā polarization configuration, respectively. The notation a(b,b)ā means the propagation direction, polarization direction of the incident light, and the polarization and propagation directions of the scattered light, from left to right in order. The scattering intensity was plotted after dividing the observed intensity by the statistical factor (n+1), where n is the Bose function. Some of the peaks are broad and asymmetric at room temperature and diverge into two, three or more peaks by the narrowing and increasing of the satellite peaks with cooling through the T_c.

The group of 284 cm^{-1} modes shows the most drastic change with temperature. The peak positions obtained by a computer fitting are plotted in Fig. 4. The bars indicate the full linewidth at half-maximum. The splitting of the line designated × in Fig. 1 is clearly seen below 200 K.

Figure 5 shows the temperature dependence of the full linewidth at half-maximum for the dominant peaks in the a(b,b)ā configuration. The apparatus linewidth is 2.5 cm^{-1}. The peaks of 160, 336, and 404 cm^{-1} are narrow even at high temperatures. Tsang et al.[8] observed the anomaly in the linewidths of the

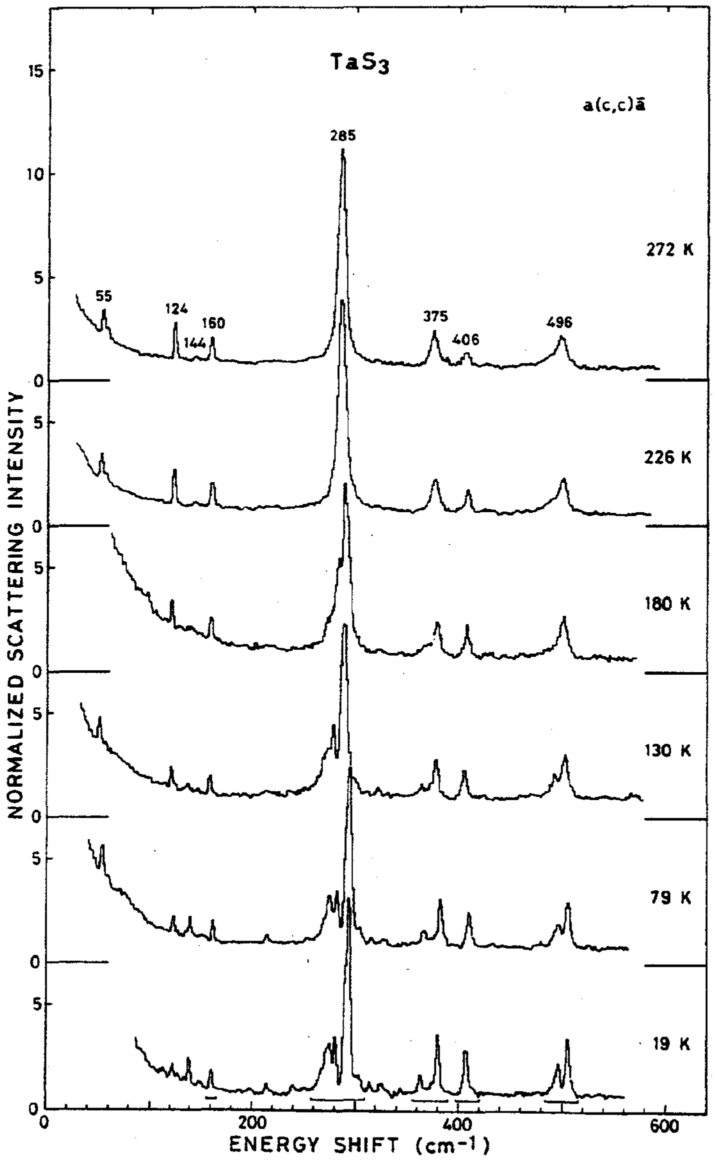

Fig. 2. Raman spectra of TaS_3 in the a(c,c)ā polarization configuration.

283, 405 and 496 cm^{-1} peaks at 200, 150 and 60 K, respectively. They estimated the CDW gap assuming the origin of the anomaly to be due to the electron-phonon interaction related to the electronic excitation through the CDW gap. However our experiment by polarized Raman scattering using a single crystal did not show such an anomaly.

As shown in Figs. 1 and 2, the satellite peaks on the lower-energy sides of the main peaks increase the relative intensity with decreasing temperature. Figure 6 shows the relative integrated scattering intensity within each group. The higher energy main peak in each group, which is dominant at high temperatures, decreases the intensity below the phase transition temperature.

III. Discussion

A. Mode assignment

A large number of atoms, as many as 96, are included in the unit cell in the normal phase. The atomic positions are not known even in the normal phase. Below T_c the unit-cell volume increases by 64 times due to the formation of the superlattice. The number of observed peaks are much less than the expected number. This implies that one broad peak consists of many peaks of the same normal modes in many chains with almost same dimensions. This idea is sup-

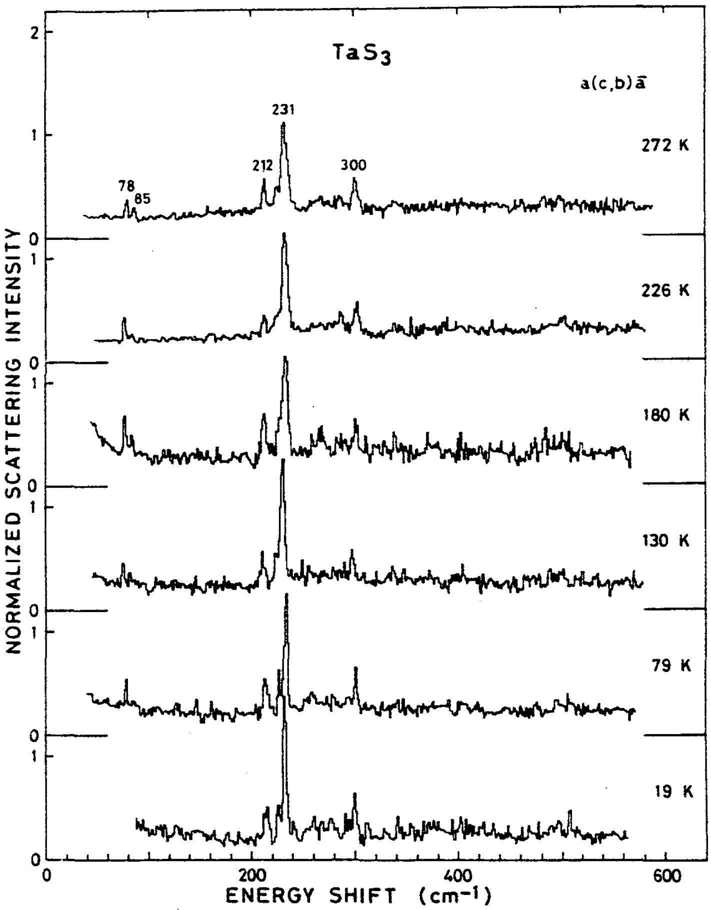

Fig. 3. Raman spectra of TaS_3 in the a(c,b)ā polarization configuration.

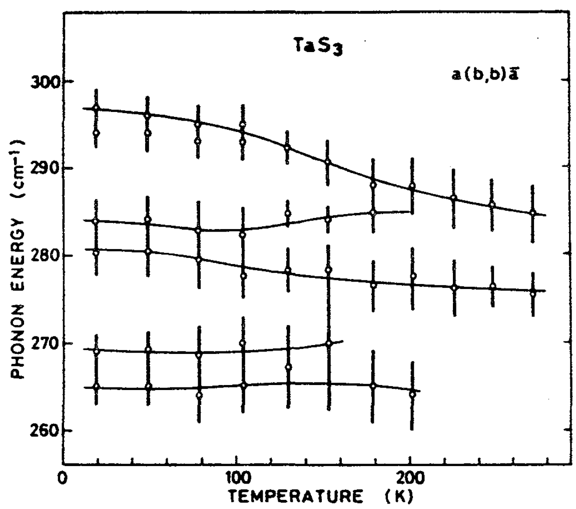

Fig. 4. Energies and full linewidths at half-maximum (indicated by bars) of the Raman peaks in the 284 cm^{-1} group.

ported from the fact that the interchain interaction is weak and the number of the chain structures is limited deducing from the monoclinic TaS_3. The monoclinic TaS_3 includes six chains in the unit cell. The chains are classified into two types of isosceles-triangular prisms with the cross sections, 2.1 × 3.6 × 3.5, and 2.8 × 3.4 × 3.4 Å approximately.[3] The peak energy 498 cm^{-1} observed in Fig. 1 is close to the energy of the S-S bond-stretching A_1 mode of the S_8 ring in the sulphur crystal and liquid.[19] The S-S bond-length in the S_8 ring, 2.048 Å, is also very close to the bond-length in one of the chains of monoclinic TaS_3.

Figure 7 shows the normal modes in the unit cell of the single isosceles-triangular chain. The A_1 and B_1 modes are active in the a(b,b)ā polarization configuration, the A_1 modes in the a(c,c)ā, and A_2 and B_2 modes in the a(c,b)ā. The 498 cm^{-1} mode is assigned to the $A_1(\nu_3)$ mode. The energy of the 284 cm^{-1} mode is very close to the 286 cm^{-1} E_{2g} mode in 2H-TaS_2. This mode is assigned to the $A_1(\nu_1)$.

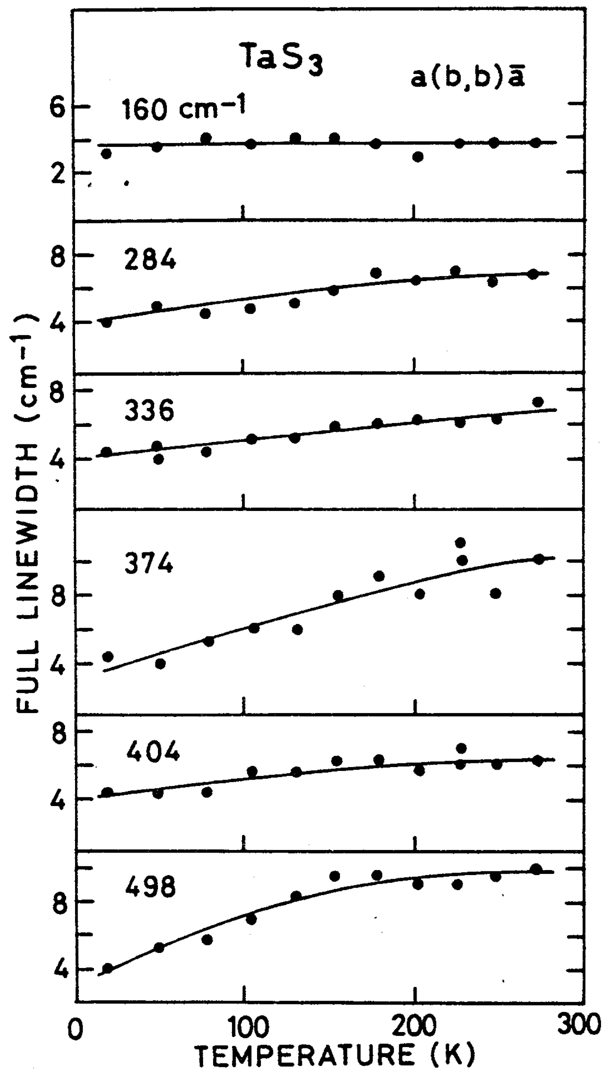

Fig. 5. Full linewidths at half-maximum of the dominant peaks in the a(b,b)ā polarization configuration.

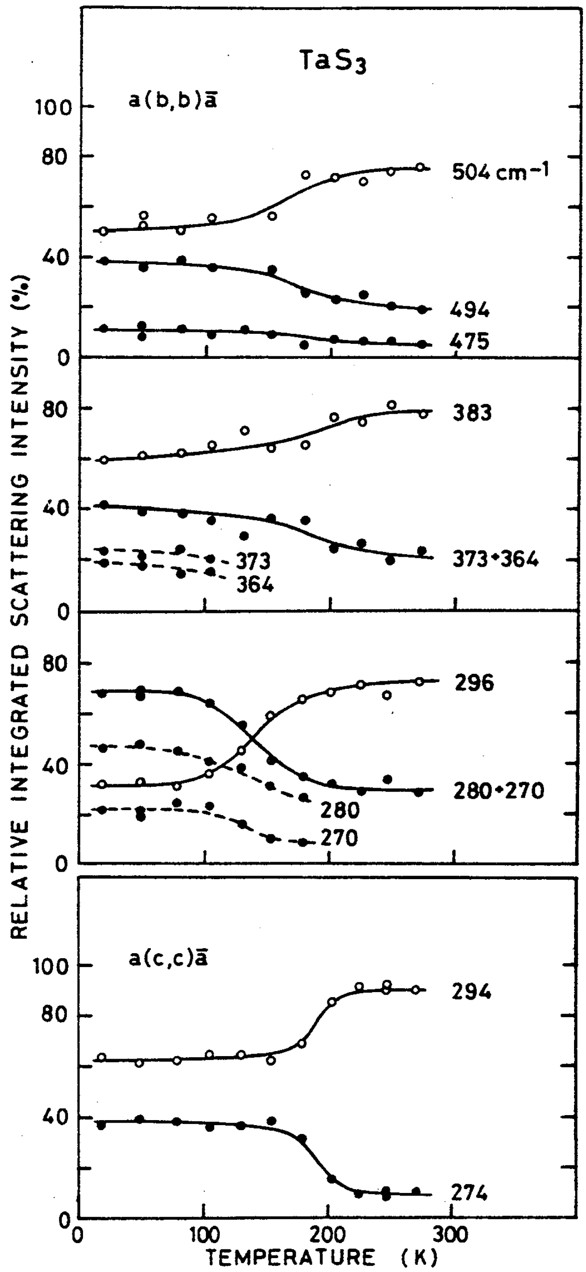

Fig. 6. Temperature dependence of the relative integrated scattering intensity within each group.

and $B_1(\nu_2)$ modes. The large change in the 284 cm^{-1} peak on temperature may be related to the atomic motion of Ta in this mode. The 374 cm^{-1} mode is tentatively assigned to the $A_1(\nu_2)$ mode. The peaks of 110 and 336 cm^{-1} are observed only in the a(b,b)ā spectra. Therefore, the 110 cm^{-1} mode is assigned to the $B_1(\nu_1)$ mode and the 336 cm^{-1} mode to the $B_1(\nu_3)$ mode. The 285 cm^{-1} peak in the a(c,c)ā configuration is assigned to the $A_1(\nu_1)$ mode. The 231 cm^{-1} peak in the a(c,b)ā spectra is tentatively assigned to the $B_2(\nu_1)$ mode.

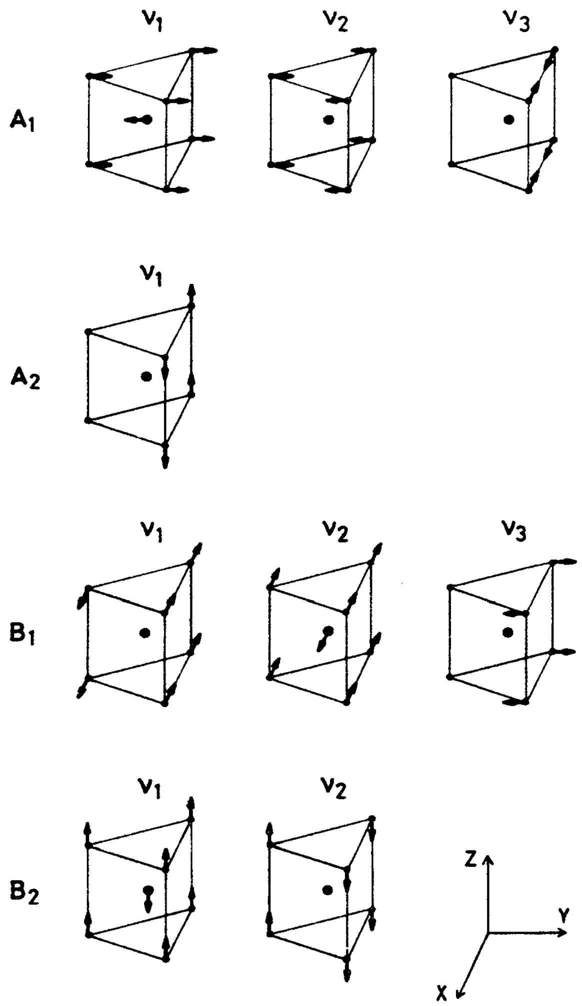

Fig. 7. Normal modes in the unit cell of the isosceles-triangular prismatic chain which is assumed to be the idealized constitutional element of orthorhombic TaS_3.

At low temperatures satellite peaks appear in the modes at 284, 336, 374, and 498 cm^{-1} in the a(b,b)$\bar{a}$ spectra, and 285, 375, and 496 cm^{-1} in the a(c,c)$\bar{a}$ spectra. Satellite peaks except one peak in the 284 cm^{-1} group appear by the narrowing and increasing the intensity in the already existing weak peaks at high temperatures keeping the energy almost constant. two mechanisms are considered for the origin of the satellite peaks. The first is that each satellite peak in a group belongs to the same normal mode in the chains with slightly different dimensions in the unit cell of the normal phase with the assumption of the weak CDW modulation. The second is that the satellite peaks belong to the normal modes of the corresponding chains in the superlattice of the CDW phase. As shown in Figs. 1 and 2, many broad peaks have the traces of the satellite peaks as asymmetric line shapes or shoulders at high temperatures, and the temperature dependence of the energies of the satellite peaks is small. Therefore we assign the satellite peaks to be due to the same normal modes of the chains in the unit cell of the normal phase. In other words the difference of the dimensions of the chains in the unit cell of the normal phase is larger than the modulation of the CDW, and the interchain interaction is small.

B. Raman scattering intensity in the materials with the CDW gap

Two mechanisms contribute to the Raman scattering intensity in metal. One is the intraband process coming from the electron-photon interaction of the $\vec{A}^2$ term[20] as shown in Fig. 8(a), where $\vec{A}$ is the vector potential. The other is the interband process due to the $\vec{P}\cdot\vec{A}$ term in Fig. 8(b). The interband process is the only important mechanism in insulating materials. In the intraband

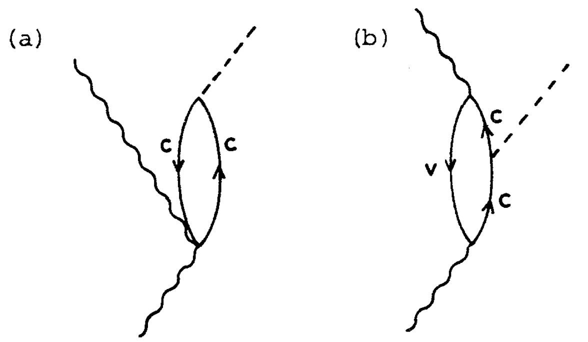

Fig. 8. (a)Intraband and (b)interband processes for Raman scattering.

process an electron is excited into the partially filled same band. In this process only the totally symmetric phonon modes are active in the parallel polarization configuration of the incident and scattered lights. The differential cross section of the intraband process is[20]

$$\left.\frac{d^2\sigma}{d\omega d\Omega}\right|_{intra} = r_0{}^2(\hat{e}_i\cdot\hat{e}_s)^2[V\chi_0(\vec{q},\omega_0)]^2(n+1) ,$$

where

$$r_0 = \frac{e^2}{mc^2} , \qquad V = \frac{G\Xi}{\sqrt{2MN\omega_0}} ,$$

and

$$\chi_0(\vec{q},\omega_0) = \sum_{\vec{k}} \frac{f(\varepsilon^c_{\vec{k}-\vec{q}}) - f(\varepsilon^c_{\vec{k}})}{\varepsilon^c_{\vec{k}-\vec{q}} - \varepsilon^c_{\vec{k}} - \omega - i\delta} .$$

Here e and m are the electron charge and mass, $\hat{e}_i$ and $\hat{e}_s$ are the polarization vectors for the incident and scattered lights, G is the absolute value of the reciprocal lattice vector, Ξ is the deformation potential, M, N, and ω_0 are the ionic mass, the total number of atoms, and the phonon frequency, respectively. n and f are the Bose and the Fermi function. Now wave vector $\vec{q}$ in the susceptibility χ_0 is small due to the momentum conservation in the Raman process. The susceptibility strongly depends on the band structure at the Fermi energy. In the approximation of low temperatures, the gradual density of states at E_F, and $\omega_0 << \varepsilon_{\vec{k}_F} - \varepsilon_{\vec{k}_F-\vec{q}}$, the susceptibility is proportional to the density of states at E_F.

The formation of the CDW gap at E_F below T_c reduces the scattering intensity from this process. As shown in Fig. 6 the higher energy peak in each group, which is dominant at high temperatures decreases the relative scattering intensity below T_c. This is explained by the decrease of the scattering probability of the intraband process due to the formation of the CDW gap. The band calculation in $NbSe_3$ shows that each one of five Fermi surfaces corresponds to each chain.[21,22] It is also the case of TaS_3. Each chain in the unit cell is

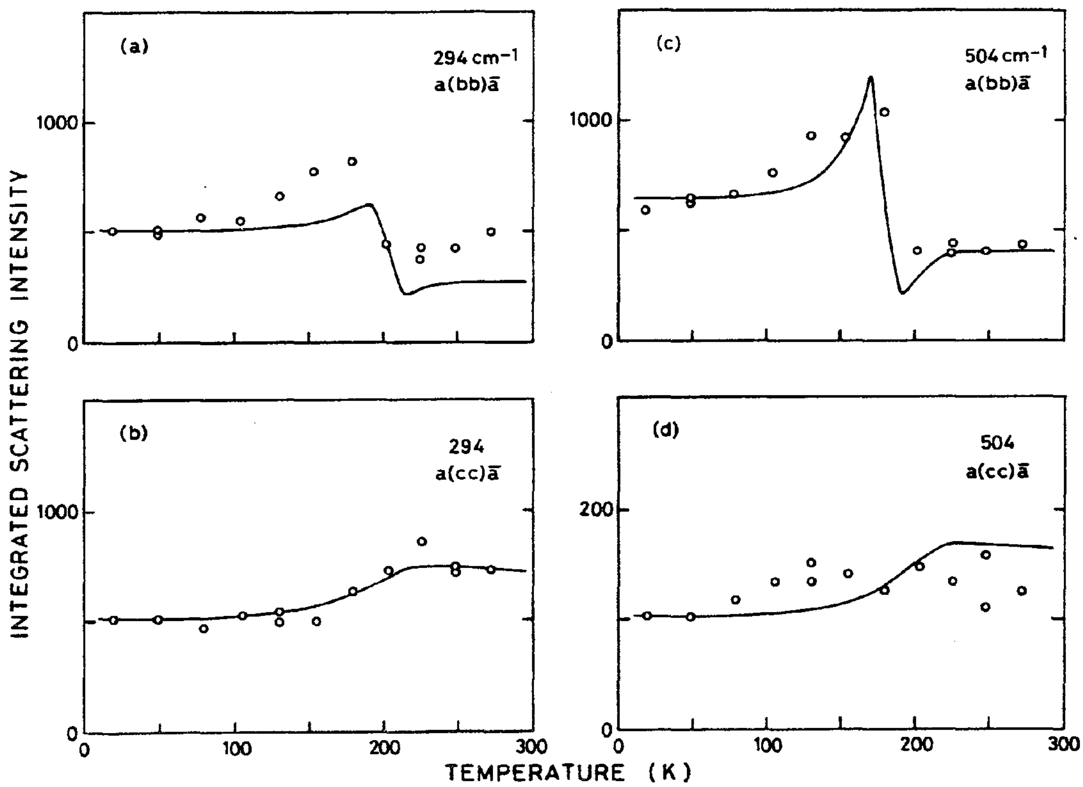

Fig. 9. Temperature dependence of the integrated scattering intensity of the highest-energy peaks in the 284 and 498 cm^{-1} groups in the a(b,b)ā and a(c,c)ā polarization configurations. Curves are calculated by the summation of the constant term for the interband process and the temperature dependent term for the intraband process. The energy gap is assumed to be 1.4 times the superconducting gap.

expected to have a different tendency for the formation of the CDW. The modes in the chains which cause the CDW transition are expected to have large Raman intensity and high energy at room temperature due to the large generalized electronic susceptibility at $2\vec{k}_F$. Such chains create a large energy gap below T_c, and the decrease in the number of free carriers reduces the intraband scattering intensity and also the screening of the atomic potential so that the phonon energy increases.

Figure 9 shows the fitting of the calculated curve to the temperature dependence of the scattering intensity of the higher energy peak in each group. The CDW gap is supposed to be 1.56 times of the superconducting gap with a transition temperature of 218 K. This amplitude of the gap has been estimated from the activation energy of the electric resistivity.[9] The different temperature dependence of the calculated curve is due to the different amplitude of the wave vector for the polarization direction, and the different mixing ratio of the intraband and interband terms.

The decrease of the scattering intensity due to the destruction of the Fermi surface in one dimensional CDW phase transition is in contrast with the two dimensional case. In 2H-$TaSe_2$ the intensity of the 240 cm^{-1} A_{1g} peak which is active in the normal phase continues to increase toward 0 K beyond the T_c.[23] The difference comes from the ratio of the destructed Fermi surface. In two-dimensional materials many areas of the Fermi surfaces remain below T_c, while the Fermi surfaces of the chains strongly related to the phase transition are supposed to be destroyed completely below T_c.

In conclusion the decrease of the scattering intensity of the higher energy main peak in each group is attributed to the decrease of the Raman cross section of the intraband process due to the formation of the CDW gap at the Fermi level with the assumption of the weak interchain interaction.

Acknowledgments

The author thanks T. Sambongi and J. Nakahara for the supply and the x-ray analysis of the TaS_3 crystals.

References

1) T. Sambongi, K. Tsutsumi, Y. Shiozaki, M. Yamamoto, K. Yamaya, and Y. Abe, Solid State Commun. 22, 729 (1977).
2) E. Bjerkelund, J. H. Fermor, and A. Kjekshus, Acta Chem. Scand. 20, 1836 (1966).
3) A. Meerschaut, L. Guemas, and J. Rouxel, J. Solid State Chem. 36, 118 (1981).
4) M. Tanaka and R. Saito (private communication).
5) K. Tsutsumi, T. Sambongi, S. Kagoshima, and T. Ishiguro, J. Phys. Soc. Jpn. 44, 1735 (1978).
6) E. Bjerkelund and A. Kjekshus, Z. Anorg. Allg. Chem. 328, 235 (1964).
7) G. van Tendeloo, J. van Landuyt, and S. Amelinckx, Phys. Status Solidi, A43, K137 (1977).
8) J. C. Tsang, C. Hermann, and M. W. Shafer, Phys. Rev. Lett. 40, 1528 (1978).
9) M. Ido, K. Tsutsumi, T. Sambongi, and N. Môri, Solid State Commun. 29, 399 (1979).
10) T. Takoshima, M. Ido, K. Tsutsumi, T. Sambongi, S. Honma, K. Yamaya, and Y. Abe, Solid State Commun. 35, 911 (1980).
11) A. H. Thompson, A. Zettl, and G. Grüner, Phys. Rev. Lett. 47, 64 (1981).
12) C. M. Jackson, A. Zettl, and G. Grüner, Solid State Commun. 39, 531 (1981).
13) A. Zettl and G. Grüner, Phys. Rev. B25, 2081 (1982).
14) A. Zettl, G. Grüner, and A. H. Thompson, Phys. Rev. B26,5760 (1982).
15) A. Zettl, C. M. Jackson, and G. Grüner, Phys. Rev. B26, 5773 (1982).
16) G. Grüner, A. Zettl, W. G. Clark, and A. H. Thompson, Phys. Rev. B23,6813

(1981).
17) A. Zettl and G. Grüner, Phys. Rev. B28, 2091 (1983).
18) A. Maeda, M. Naito, and S. Tanaka, Solid State Commun. 47, 1001 (1983).
19) D. W. Scott, J. P. McCullough, and H. F. Kruse, J. Mol. Spectrosc. 13, 313 (1964).
20) P. M. Platzman and N. Tzoar, Phys. Rev. 182, 510 (1969).
21) N. Shima, J. Phys. Soc. Jpn. 51, 11 (1982).
22) N. Shima, J. Phys. Soc. Jpn. 52, 578 (1983).
23) S. Sugai and K. Murase, Phys. Rev. B25, 2418 (1982).